and d) are zero at roll rate. 3) Small trim angles of attack ($\bar{\zeta}_T \leq 0.25°$), which can be produced by principal axis inclination angles of similar magnitude, may seriously degrade the performance of re-entry vehicles that have mass asymmetries. 4) Effects of inertia asymmetries on the angular and rolling motions of ballistic re-entry vehicles may be misinterpreted as the effects of mass and aerodynamic asymmetries.

References

[1] Pettus, J. J., "Persistent Re-Entry Vehicle Roll Resonance," AIAA Paper 66-49, New York, Jan. 1966.

[2] Glover, L. S., "Effects on Roll Rate of Mass and Aerodynamic Asymmetries for Ballistic Re-Entry Bodies," *Journal of Spacecraft and Rockets*, Vol. 2, No. 2, March–April 1965, pp. 220–225.

[3] Barbera, F. J., "An Analytical Technique for Studying the Anomalous Roll Behavior of Re-Entry Vehicles," *Journal of Spacecraft and Rockets*, Vol. 6, No. 11, Nov. 1969, pp. 1279–1284.

[4] Nicolaides, J. D., "Missile Flight and Astrodynamics," TN 100A, 1959–61, U.S. Bureau of Weapons, Dept. of the Navy, Washington, D.C.

[5] Vaughn, H. R., "Boundary Conditions for Persistent Roll Resonance on Re-Entry Vehicles," SC-RR-67-287, May 1967, Sandia Labs., Albuquerque, N. Mex.

[6] Carlson, R. W. and Louis, C. A., III, "Introduction to Re-Entry Flight Dynamics," LMSC-D050690, March 1968, Lockheed Missiles & Space Co., Sunnyvale, Calif.

[7] Hodapp, A. E., Jr. and Clark, E. L., Jr., "A Technique for Determining Approximate Roll Rate Histories for Ballistic Re-entry Vehicles Having Mass, Inertia, and Aerodynamic Asymmetries," SC-RR-69-804, Sept. 1970, Sandia Labs., Albuquerque, N. Mex.

[8] Platus, D. M., "A Simple Analysis of Re-Entry Vehicle Roll Resonance," TR-1001(2240-30)-10, Jan. 1967, Aerospace Corp., El Segundo, Calif.

[9] Hodapp, A. E., Jr. and Clark, E. L., Jr., "The Effects of Products of Inertia on the Roll Behavior of Ballistic Re-Entry Vehicles," AIAA Paper 70-204, New York, Jan. 1970.

[10] Fail, R. and Garner, H. C., "Calibration Models for Dynamic Stability Tests," Rept. 563, 1968, Advisory Group for Aerospace Research and Development, Neuilly-sur-Seine, France.

[11] Ward, L. K., Jr. and Hodapp, A. E., Jr., "A Three-Degree-of-Freedom Dynamic Stability Balance for Use in the VKF Continuous Flow Hypersonic Tunnels ($M_\infty = 6$ through 12)," AEDC-TR-68-62, May 1968, Arnold Air Force Station, Tenn.

FEBRUARY 1971 J. SPACECRAFT VOL. 8, NO. 2

An Exploratory Study of the Roll Behavior of Ablating Cones

JOHN B. MCDEVITT*
NASA Ames Research Center, Moffett Field, Calif.

The coupling between roll dynamics and ablation patterns on cones has been investigated in the NASA Ames 3.5-Foot Hypersonic Wind Tunnel. A gas-bearing apparatus, which allowed the test models to be free in roll, was used to obtain the roll characteristics of a series of models exhibiting various ablation patterns (a basically subliming ablator and one involving a melt layer were used). Streamwise vortex grooving, turbulent wedge erosion, and cross-hatching were obtained by choosing suitable combinations of cone vertex angle and ablation material, and it was found that any of these patterns can introduce roll torques. For a subliming ablator, the direction of initial spin did not appear to bias the results, and reversals in torque direction were common. For a melting ablator it was found that torque in the direction of spin can also occur for the smooth cone if the model is rolling at angle of attack.

Nomenclature

A_b,d = model base area and diameter
C_l = rolling moment coefficient, $L/q_\infty A_b d$
C_{lp} = roll damping derivative, $\partial C_l/\partial(pr_b/U_\infty)$
h_0,h_1,n = shape change parameters, Eq. (A2)
I_x = moment of inertia about cone axis
$K_{\text{tare}},K_{\text{aero}}$ = constants, Eqs. (1) and (2)
L = rolling moment
l = cone length
M_∞ = freestream Mach number
$m/\rho_\infty U_\infty A_b$ = normalized ablation rate, (ρ_∞ = freestream density)
P,P_{t_1} = static and total pressures, respectively
p,φ = roll rate, rad/sec
$\dot{p},\ddot{\varphi}$ = roll acceleration, rad/sec^2
q_∞ = freestream dynamic pressure
r_b = base radius of cone
T_t = total temperature
t = time
U_∞ = freestream velocity
W = weight of model
x = axial distance from cone apex
y,z,θ = cylindrical coordinate system, Fig. 15
$\bar{y},\bar{z}$ = coordinates of the center of gravity for an ablating model
α,β = angles of attack and sideslip, respectively
λ = angle between crossflow velocity vector and horizontal plane of tunnel, Fig. 15
σ_c,θ = cone semivertex and azimuthal angles, respectively
φ = roll angle
$(\ )_0$ = at $p = 0$ or $t = 0$
$(\ )_\infty$ = freestream condition

Presented as Paper 70-562 at the AIAA Atmospheric Flight Mechanics Conference, Tullahoma, Tenn., May 13–15, 1970; submitted May 25, 1970; revision received October 22, 1970.

* Research Scientist. Member AIAA.

Introduction

WILLIAMS[1] demonstrated that roll torques can develop for ablating cones, but his study was confined to static measurements using a strain-gage, flexural-pivot balance. The present paper describes a study wherein a gas-bearing apparatus, which allowed the test models to be free in roll, was used to obtain the roll characteristics of a series of models as they developed various ablation patterns that are identifiable with certain ablation-flow interaction phenomena.

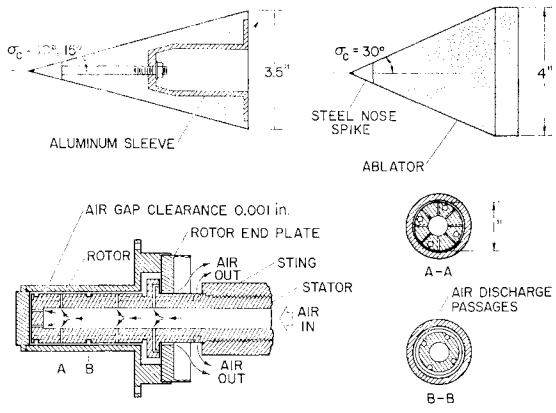

Fig. 1 Schematics of test models and gas bearing.

The past studies of surface ablation patterns sensibly began with investigations by Chapman et al. of certain meteorites that exhibit "ring wave" and "regmaglypt" features.[2,3] The discovery of diamond-shaped ablation patterns (commonly referred to as cross-hatching) on recovered flight vehicles prompted numerous experimental studies[4–10] in ground-based facilities. Larson and Mateer, in tests in the Ames 3.5-Foot Hypersonic Wind Tunnel, demonstrated two of the requirements for cross-hatching—a turbulent boundary layer and local supersonic flow.[6,8] A summary of experimental observations of the cross-hatching phenomenon is included in Ref. 10.

The frequent appearance of longitudinal grooves upstream of cross-hatched patterns suggests a relationship between streamwise vortices and pattern development, and such a theoretical model for the origin of cross-hatching has been offered by Tobak.[11] However, relatively little attention has been directed toward the study of longitudinal-groove pattern development, although a recent experimental study[12] of the effect of streamwise vortices on ablation groove formation demonstrated that upwash due to angle of attack can have a pronounced effect on the shape changes due to ablation. Another pattern of interest is the turbulent wedge phenomenon, where local regions of greatly increased ablation rates lead to prominent shape changes.[4,5]

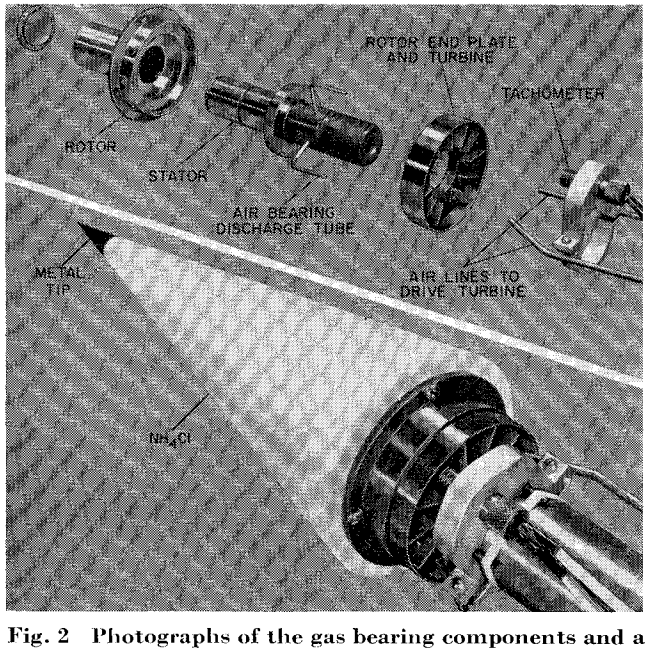

Fig. 2 Photographs of the gas bearing components and a typical NH_4Cl test model.

The three ablation features of interest for the present study were streamwise grooves, turbulent wedge erosion, and cross-hatching. Each of these patterns has been obtained by using suitable combinations of cone vertex angle and ablation material.

Facility, Models, and Apparatus

The tests were conducted in the Ames 3.5-Foot Hypersonic Wind Tunnel at $M_\infty = 7.4$, $P_{t_1} = 102$ atm, and at nominal total temperatures of 2000° R, which provide a nominal freestream Reynolds number of 4.5×10^6/ft. The tunnel used is a pebble-bed heated, blowdown-type facility utilizing interchangeable, contoured nozzles that provide nominal Mach numbers of 5, 7.5, and 10. A quick-insert mechanism permits insertion of the model into the test section after the tunnel reaches preselected, steady-state stream conditions, and retraction before the tunnel is shut down.

The test models (Figs. 1 and 2) consisted of solid metal cones and ablating models made of ammonium chloride, camphor, and Special Korotherm (a material used previously by Williams).[1] The Korotherm material was cast about the aluminum sleeve (which provides a sliding fit with the gas-bearing rotor). The NH_4Cl and camphor models were made by sintering powdered material over the aluminum sleeve under high pressure (4200 psi), inserting the metal nose spikes, and machining the conical surface. To limit the aerodynamic loads to values compatible with the capacity of the gas bearing, the maximum diameter of the larger angle cone was restricted to 4 in., leading to the cone-cylinder design shown in Fig. 1.

The one-degree-of-freedom (roll) gas bearing designed for the present investigation consists basically of independent (in that the gas discharged from one load supporting air cushion does not interfere with other bearing regions) load-supporting regions—separate forward and rearward thrust bearings and two adjacent, normal-force bearings. The stator (Fig. 1) was made of stainless steel, the rotor from mild steel with a very thin coating of nickel. Rotor air-gap clearances of 0.0005 and 0.001 in. gave satisfactory results. The diameter of the gas supply ports to the load-bearing surfaces was 0.05 in. The original design included an air-driven turbine attached to the rotor base for prespinning the model in either direction (Fig. 2). The roll rate p was monitored by a magnetic tachometer mounted so as to respond to the passage of each turbine vane and by motion pictures (colored strips were painted on the exposed portion of the rotor to aid in reading the film). This type of roll sensor proved to be awkward to use, since the signal strength is proportional to the roll velocity and also has the undesirable effect of introducing some roll damping (although the effect is small) as a result of electrical induction. Figure 2 also shows a slender NH_4Cl model mounted on the air bearing and with the magnetic tachometer installed. This arrangement was used for the first part of the investigation (roll tests of 15° ablating cones). Following the initial tests the magnetic tachometer was replaced by a photodiode device, which proved to be an ideal way to monitor p.

The modified apparatus was used in the second half of this study for the 30° ablating cones. A miniature, 6-v bulb was used as the light source and the silvered ends of small, right-circular cylinders, embedded in the rotor end plate, served to reflect the light. Two sensors were incorporated, one providing 12 signals per revolution (not used in the present tests) and one with 36 signals per revolution. The output from the photodiode was amplified and recorded on an oscillograph. A frequency meter was also incorporated and monitored visually during the test runs, and its pulsed output was recorded, as was the strut position of the quick-insert mechanism. Since the illumination from the light source was nonuniform, the recorded signal output from the

photodiode had characteristic shapes for clockwise (base view of the model, looking upstream) and counterclockwise rotations (Fig. 3); thus the direction of roll, at least for small roll velocities, could be deduced from the oscillograph records, as well as from the motion pictures.

Static tests indicated that, for a supply pressure of 100 psi (air) to the gas bearing, axial, and normal forces of about 30 lb could be supported. A supply pressure of 150 psi was used for the tests of the 15° cones and 250 psi for the 30° cone models.

An undesirable feature of the gas bearing was a small driving torque introduced by internal flow. During the initial use of the bearing (with the 15° cone models), it was determined that for a supply pressure of 150 psi, this torque was about 4×10^{-4} lb-ft at $p = 0$ but decreased with increasing p. To minimize this torque, all internal surfaces (not just the load-bearing regions) were polished, and all gas-supply and discharge passages were symmetrically located. The torque was thus reduced about an order of magnitude, but not completely eliminated (for reasons which were not understood).

Aerodynamic Roll Damping Measurements

Before starting the roll tests of the ablating 30° cones, a metal (nonablating) cone was used to evaluate the gas-bearing performance under relatively large aerodynamic loads and to obtain, if possible, aerodynamic damping data for the nonablating case for reference. Prerun tare measurements, reflecting the internal torque of the bearing, are presented in Fig. 4 for angles of attack (α) of 0°, −2.5°, and −5°. The tare moments can be approximated as

$$L_{\text{tare}} = (L_{\text{tare}})_0 + K_{\text{tare}} I_x p \qquad (1)$$

The residual moment $(L_{\text{tare}})_0$ varied considerably between runs, but the slopes of the data, represented by K_{tare}, remained essentially constant at $K_{\text{tare}} \approx -0.004$ (an extrapolated result for $P_\infty \to 0$).

Roll damping was measured for both positive and negative spin rates during the same run (utilizing the base turbine device, Fig. 2, to change spin rates and directions between data acquisitions) and the average values for roll acceleration,

$$\dot{p}_{av} = \tfrac{1}{2}[(\dot{p})_{\text{positive spin}} - (\dot{p})_{\text{negative spin}}]$$

are shown on the lower left-hand side of Fig. 4. Taking the average reading effectively eliminated the influence of $(L_{\text{tare}})_0$ (in fact, this quantity need not be evaluated). However, the tare slope, represented by K_{tare}, must be accounted for. The corrected data, where $K_{\text{tare}} p$ has been subtracted, are shown on the lower right-hand side of Fig. 4. At the lower roll rates, the effect of α is small, and within the accuracy of the tests, a damping derivative C_{l_p} of

$$C_{l_p} = I_x(\dot{p}/p)/\rho_\infty U_\infty r_b{}^4 \pi = 6.9 \times 10^{-3}$$

is indicated. If the aerodynamic damping can be represented by a linear system (usually valid for small roll rates),

$$L_{\text{aero}} = (L_{\text{aero}})_0 - K_{\text{aero}} I_x p \qquad (2)$$

the aerodynamic damping factor may be obtained directly from

$$K_{\text{aero}} = K_{\text{tare}} - \tfrac{1}{2}[(\dot{p}/p)_{\text{positive spin}} - (\dot{p}/p)_{\text{negative spin}}]$$

where, in the linear case, it is not necessary for the absolute values of the two spin rates to be equal.

Results and Discussion

Streamwise grooves are believed to be the result of streamwise (Görtler) vortices. In Ref. 12 evidence of vortex arrays was noted for 10° and 15° cones at angle of attack, but not

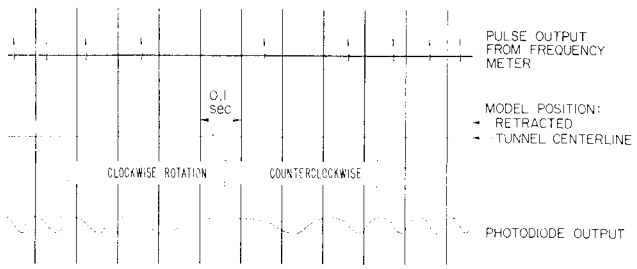

Fig. 3 Sample oscillograph record showing roll reversal.

at $\alpha = 0°$, and for ablating cones having sharp nonablating tips followed by rearward-facing steps (arising during ablation) at $\alpha = 0°$ as well as at $\alpha > 0°$. Evidence of similar vortex arrays has been noted in the past for flows over swept-back wings and following flow separation caused by various types of steps or ramps on planar and axisymmetric bodies.[13,14] Ginoux[13] studied the flow behind a step using a sublimation technique to display the regular striation patterns believed to be due to counterrotating pairs of vortices. His detailed surface heat transfer and flowfield pitot surveys showed large peaks in the spanwise distributions of heating and pitot pressure at locations compatible with the sublimation pattern. Thus, it is reasonable to assume that the presence of longitudinal ablation grooves is consistent with the presence of streamwise vortices.

15° NH_4Cl Cones

In the first test, at $\alpha = 0°$, the model, initially at rest, was disturbed slightly during insertion into the tunnel (an insertion elapsed time of 1 sec was chosen, and the test time was measured from the instant the model reached the tunnel centerline). The roll motion introduced by the insertion process arises from two factors: first, the effect of acceleration if the model mass center is not alined with the bearing axis (a very small effect for the model design used here); and second, a mass asymmetry introduced when the model traverses the varying heating environment of the tunnel boundary layer. For this test, the initial disturbance was small, and $p \simeq 0$, until $t \simeq 20$ sec (Fig. 5), whereupon the model suddenly took on the motion of a compound pendulum with rotational amplitude of about ±120°. This motion is the result of a sudden shift in the model mass center, caused either by mass lost when foreign particles impinged on the model (the test facility's pebbled-bed heater introduces some dust) or by the sudden growth of a turbulent-wedge region. The pendulum motion was replaced at about $t = 55$ sec by a spin-up motion, indicating the appearance of a surface roll torque, which had the approximate value $C_l = I_x \dot{p}/q_\infty A_b d = 1.2 \times 10^{-5}$.

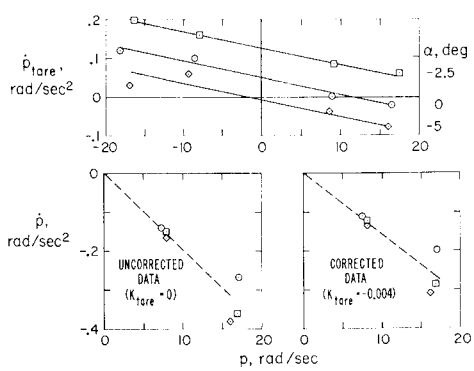

Fig. 4 Tare data (top, wind off, $P_\infty \approx 0.25$ psi) and aerodynamic damping of a nonablating 30° cone; $M_\infty = 7.4$, $R_{\infty,l} = 2.6 \times 10^6$.

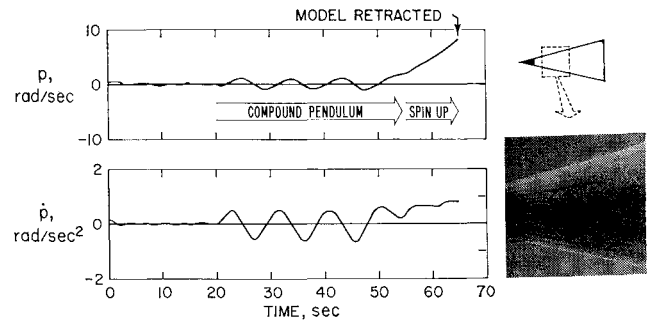

Fig. 5 Roll test of an albating NH_4Cl, 15° cone at $\alpha = 0°$.

Prominent streamwise vortex grooves, emanating from the base of the metal tip and terminating near midlength of the model, were present after the run. The greatest mass removal appeared to be in the region immediately downstream of where the vortex grooves disappear and one prominent turbulent wedge feature was observed (see photograph in Fig. 5). The absence of surface torques for the first 55 sec of the run indicates that streamwise vortex grooves are probably not a significant factor in producing surface torques. However, the breakdown of the vortices and/or the formation of localized turbulent wedges, where significant lateral growth of the disturbances is involved, may introduce surface torques. The turbulent wedge phenomena can also be expected to introduce noticeable mass asymmetries when the turbulent region, originating from a roughness element or surface imperfection, is surrounded by laminar or transitional flow.

The next phase of the study involved roll tests of 15° NH_4Cl cones at a sideslip angle β of 5° (model yawed 5° in the horizontal plane, nose to the left when looking upstream; see Fig. 6). In this orientation the uneven circumferential ablation rate due to the angle of yaw results in mass asymmetry, and thus a weight torque due to gravity is to be expected (the effect of mass asymmetry on roll torque for sting-mounted test models will be discussed in some detail later in this paper). The first test result is presented at the top of Fig. 7 (run 1). Here the model was inserted into the tunnel stream with a zero initial roll rate, but the model responded rapidly to the weight torque introduced by the uneven ablation and the tare roll moment generated internally by the gas bearing (see discussion in preceding section). The decrease in roll rate after about 30 sec is due to a marked increase in aerodynamic damping as the surface became rough. After the run there was no evidence of longitudinal grooves (except near the metal tip), and this is to be expected since the crossflow due to α is time-dependent in body coordinate systems for rotating models. For run 2 in Fig. 7, torques were applied to the model as indicated in the figure (dashed lines), and the model was then allowed to spin freely. The spin motion ceased at 30 sec; the model then underwent a

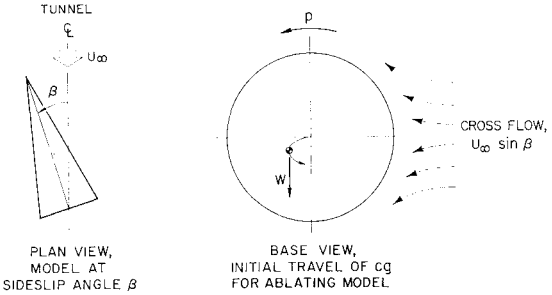

Fig. 6 Effect of sideslip angle on instantaneous cg location for an ablating cone.

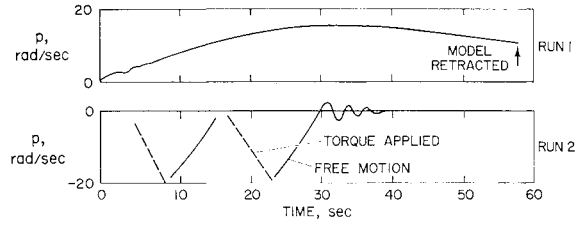

Fig. 7 Roll tests of ablating NH_4Cl, 30° cones at 5° sideslip angle.

rapidly damped pendulum-type motion, converging toward a fixed ("locked-in") roll orientation, even though the mass asymmetry was growing steadily. An attempt was then made, before the end of run 2 (i.e., before removing the model from the tunnel stream), to spin the model by applying air to the turbine, but this could not be accomplished; in fact, the roll orientation could only be changed by a few degrees. Inspection of the model after the run showed pronounced upwash groove patterns (similar to those shown in Ref. 12).

Several additional runs, similar to run 2, produced the same model roll behavior, and the models all exhibited upwash erosion patterns and pronounced mass asymmetries due to the higher ablation rates on the windward surface when at the nonspinning, "locked-in" orientation. The roll stability in this orientation is believed to result from two factors: the upwash grooves probably provide some weathervane stability, and the larger surface recession rate on the windward surface causes the center of pressure, originally at the cone axis, to shift in the leeward direction, thus introducing positive aerodynamic roll stability.

30° NH_4Cl Cones

Motion pictures of the ablating 30° NH_4Cl cones showed longitudinal striations appearing almost immediately but cross-hatching only after about 15–20 sec (Fig. 8). This sequence in ablation pattern formation is fortunate in that the roll behavior in the presence of longitudinal vortex grooving could be observed first, and then the effect of the onset of cross-hatching. The use of nonablating tips served to keep the Reynolds number and Mach number high, and the rearward-facing step arising during ablation enhanced the formation of longitudinal vortices. However, it is not known whether the step, vortex-array phenomenon was instrumental in starting the cross-hatching observed on the 30° cones, or merely contributed to early turbulent flow.

A self-blunting model (no metal tip) was also tested at $\alpha = 0°$, but no ablation patterns were observed. The model was then reshaped to have a slight concavity, hoping to introduce vortices by the surface curvature, but again the blunt tip effect dominated, except downstream of a cavity near the nose, which appeared suddenly during the test (see postrun photographs in Fig. 8). Downstream of this cavity, streamwise grooves are evident, and incipient cross-hatching is observed. It is interesting to note that, again, longitudinal grooves preceded the cross-hatching.

Figure 9 shows timewise mass losses (initial weights were near 530 gm). For the metal-tipped models, the ablation rate increases after the onset of cross-hatching. For a self-blunting model, which remained smooth throughout the test, the mass loss is relatively low, occurring mostly at the nose.

The roll behavior of four 30° NH_4Cl cones tested at $\alpha = 0°$ is presented in Fig. 10. For run 1 the model was inserted with $p_0 = 0$, but it began rotating at about 3 rad/sec due to a slight mass asymmetry resulting from the insertion process (traversing the tunnel boundary layer). Aerodynamic damping is evident until about 20 sec have elapsed, whereupon p increases rapidly as the cross-hatching patterns be-

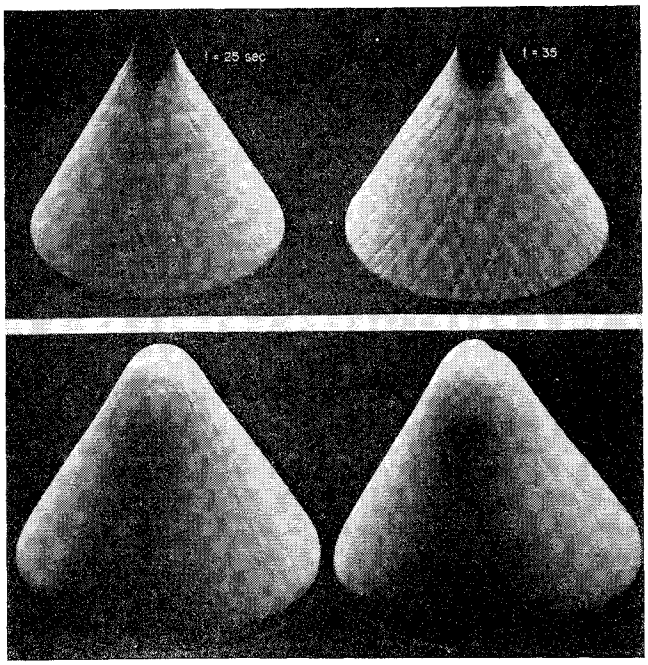

Fig. 8 Postrun photographs of ablated metal-tipped NH_4Cl, 30° cones (top) and self-blunting NH_4Cl, 30° cones (bottom).

come noticeable. Since the spin-up roll direction was the same as that before the appearance of cross-hatching, the next runs (2–4) were made with models prespun in the opposite direction. These runs made it clear that the initial spin direction does not bias the results; in fact, in run 4 a roll reversal phenomenon is indicated. During all four runs, rapid changes in p occur shortly after the appearance of cross-hatching, and torque coefficients $I_x\dot{p}/q_\infty A_b d$ ranged from 10^{-5} to 10^{-4}. The slopes of the curves are often constant, or nearly so (indicating essentially constant torque values) for several seconds at a time. Changes in torque values are often quite abrupt. (Tests of nonablating models produced no examples of spin-up torques, but only the expected aerodynamic damping.) The ablated models used in runs 1–3 were later rerun, and the results are presented on the right-hand sides of Figs. 10a-c. In each case the initial roll behavior during the first few seconds of the rerun was compatible with the model behavior at the time the original run was terminated (model retracted from the test section).

The roll histories of four runs at $\alpha = -2.5°$ are presented in Fig. 11, and the histories of two runs at $\alpha = -5°$ are shown in Fig. 12. Negative pitch angles were chosen for these tests since this is the only orientation for which ablation mass asymmetry due to α in the static case (no roll) introduces positive stability, and thus interpretation of the dynamic roll tests was facilitated. Two models started with $p_0 = 0$, runs 1 and 4 of Fig. 11, but were disturbed by the insertion process. The remaining models were prespun to various p_0's. All models experienced aerodynamic damping during the early portions of the runs, but in all cases a spin-up behavior was noted before the end of each run. The postrun appearances of the models were similar to that shown in the photograph of Fig. 8 for the metal tipped model tested for 35 sec.

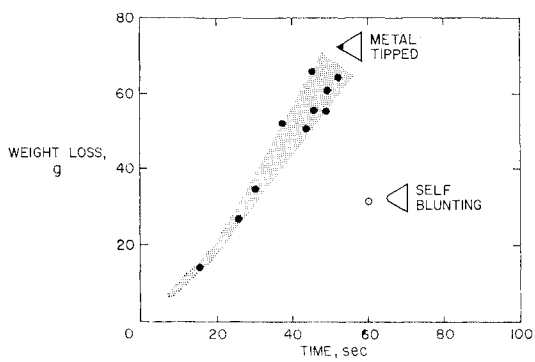

Fig. 9 Ablation mass loss of 30° NH_4Cl cone models, $T_t \approx$ 2000°R.

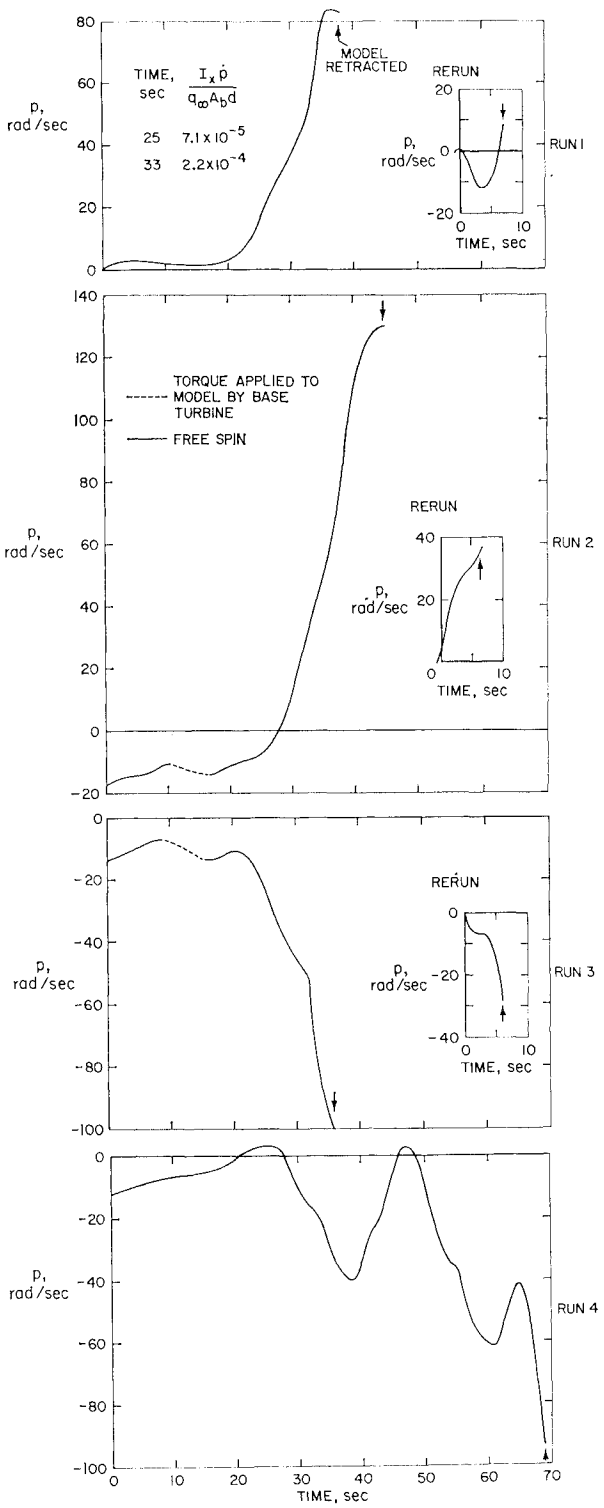

Fig. 10 Roll behavior of ablating 30° NH_4Cl cones ot α = 0°.

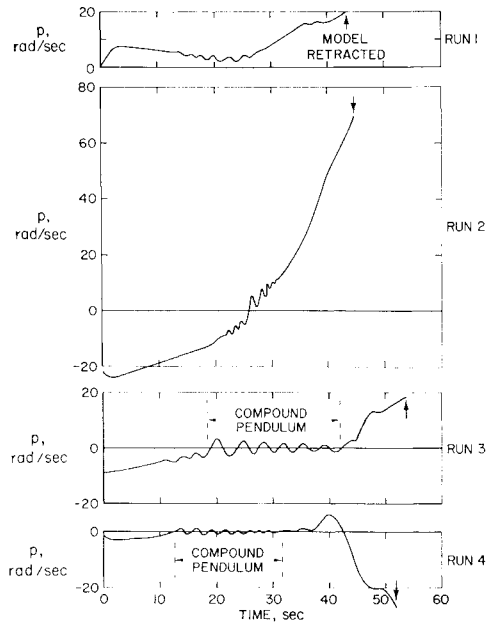

Fig. 11 Roll behavior of ablating 30° NH_4Cl cones at $\alpha = -2.5°$.

In contrast to the four models tested at $\alpha = 0°$, where strong surface torques occurred almost exactly at the same test time ($t \approx 25$ sec) in each case, the occurrence of surface torques in the angle-of-attack case was erratic, appearing as early as about 27 sec but usually delayed to the interval between 35 and 45 sec. The test results at angle of attack also exhibit, at small roll rates, small oscillatory motions superimposed on the general motion, a phenomenon not evident in the $\alpha = 0°$ tests. In some cases, as labeled in Figs. 11 and 12, the motion is that of the compound pendulum, introduced by mass asymmetry. However, a coupling between local ablation irregularities and the stream cross flow induced by the angle of attack is also a contributing factor. For instance, the turbulent wedge depressions are primarily the result of vortex action. The positions and strengths of the vortices are probably highly sensitive to the local stream

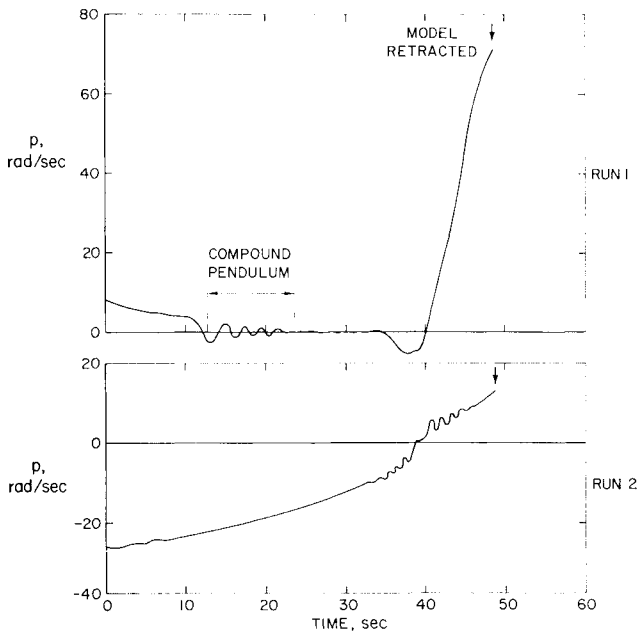

Fig. 12 Roll behavior of ablating 30° NH_4Cl cones at $\alpha = -5°$.

direction, which is influenced by an azimuthally varying cross flow component when the cone is rolling at angle of attack (see discussion of the cross-flow phenomena in Ref. 12).

Korotherm Cones

Three 30° cones made of Korotherm were tested on the gas bearing, two models at $\alpha = 0°$ and one at $\alpha = -5°$. The roll histories of these ablating models are displayed in Fig. 13. Typical postrun photographs are presented in Fig. 14. In contrast to NH_4Cl, which appeared to ablate by sublimation only, Korotherm ablates with a thin liquid layer, which appears within a few seconds after the model is inserted into the stream and flows rearward, interacting momentarily with the stream to form moving oblique wave patterns. The latter phenomenon, analyzed by Nachtsheim,[15,16] persists for only a few seconds and disappears as the melt layer thickens. Motion pictures also show the start of numerous turbulent wedges that deepen and grow laterally into the prominent features displayed by the postrun photographs. Finely spaced longitudinal grooves are also displayed (see Fig. 14) as well as the beginning of relatively wide-spaced oblique features (the appearance is suggestive of vortex actions) believed to be incipient cross-hatching.

Both of the models tested at $\alpha = 0°$ underwent low amplitude oscillations of the compound pendulum mode, introduced by mass asymmetries (the turbulent wedge phenomenon is, of course, a strong mechanism for unbalancing the model). Both models eventually spun up, shortly after the onset of cross-hatching, first noticeable within the turbulent wedge regions.

The model tested at $\alpha = -5°$ was prespun to about 9 rad/sec. The oscillatory motion superimposed on the general motion for the first part of the run results from uneven model heating during insertion into the tunnel. Note, however, the steady increase in the mean p from $t = 2$ sec to $t = 18$ sec, indicating a steady torque in the direction of spin. The behavior of this melting model is in marked contrast to the behavior of the subliming NH_4Cl models at $\alpha = -2.5°$ and $-5°$, which all indicated, without exception, aerodynamic damping early in the runs. At about 20 sec into the run, turbulent wedge depressions had appeared and the roll motion damped rapidly to a small oscillation about $p = 0$. For the nonrolling model, the differential ablation rates due to α lead to shape changes where the center of pressure moves in the direction of the crossflow, and thus static roll stability is introduced. Some weathervane type of roll stability due to the effect of crossflow on ablation pattern development may also be involved; in any event, the model exhibited roll stability during the rest of the run and, although cross-hatched features are evident on the windward side, the surface torques were not of sufficient magnitude to disturb the model from its locked-in roll orientation.

Concluding Remarks

The present tests of sharp ablating cones resulted in a variety of surface patterns involving, in particular, longitudinal grooves, turbulent wedges, and cross-hatching. The study of the coupling between roll dynamics and ablation indicated that any of the features mentioned can introduce roll torques, particularly when the phenomenon leading to cross-hatching is present.

In the case of the orderly array of streamwise vortices, the ablation grooves are aligned with the stream, and significant lateral aerodynamic forces are not to be expected. However, in the downstream regions where the array of vortices is being replaced by more or less fully developed turbulent flow, with turbulent-wedge regions present, roll torques can arise. Similarly, when the early growth of surface erosion behind a roughness element is confined to a narrow strip, roll torques are probably not significant, but when the turbulent-wedge

is characterized by a laterally spreading channel a fine balance in lateral components of fluid momentum cannot be expected. Not only can the local flow over the oblique leading-edge steps depart significantly from conical flow, but the formation of cross-hatching within the wedge region is possible, creating additional oblique channels.

The cross-hatching phenomenon is a complete departure from the streamwise orientation of the striations, involving two families of oblique crisscrossing channels and invariably producing roll torques. In the present tests with a subliming ablator (the 30° NH_4Cl cones where a liquid or melt layer did not appear to be involved) cross-hatching occurred at angle of attack ($-2.5°$ and $-5°$) as well as at 0° angle of attack, and the magnitude of the roll torque coefficients associated with the appearance of the cross-hatching ranged from 10^{-5} to 10^{-4}. The direction of initial spin did not appear to bias the results, and reversals in torque directions were common (complete roll reversals occurred in some cases). The use of an ablator with a melt layer indicated that liquid-layer run off tends to suppress the cross-hatching phenomenon, in agreement with the findings of Nachtsheim.[15-16] However, a roll torque in the direction of spin occurs for the smooth cone with liquid-layer runoff when the model is rolling at angle of attack.†

Another general finding was that for ablating cones that do not cross-hatch (the 15° NH_4Cl cone models), the differential ablation rates due to angle of attack for the nonrolling model introduce a relatively high degree of roll stability. This stability is due to a favorable shift in the center of pressure as the shape departs from the circular cross section, and some weathervane stability may be involved if upwash grooves are present.

Appendix: Effect of Model Weight Torque on Roll

Since uneven ablation rates on windward and leeward surfaces cause a movement of the center of gravity from the original axis of symmetry, a roll torque due to gravity is introduced (Fig. 15). The component of freestream velocity normal to the cone axis at the most windward meridian has the value $U_\infty \sin(\alpha^2 + \beta^2)^{1/2}$ and the crossflow vector intersects the horizontal plane of the tunnel with angle λ. The particular case of $\alpha = 0$ and negative sideslip (model yawed nose to the left) is represented by $\lambda = 0$. For negative α but $\beta = 0$, $\lambda = \pi/2$, etc.

The instantaneous center of gravity for the ablating model has coordinates $\bar{y},\bar{z}$ and the resulting torque due to gravity is

$$L_{\text{gravity}} = W\bar{z}\sin\lambda - W\bar{y}\cos\lambda$$

For the present analysis, the aerodynamic damping is assumed to vary linearly with roll velocity

$$L_{\text{aero}} = -C_{l_p}(q_\infty A_b d)pr_b/U_\infty = -K_{\text{aero}}p$$

Aerodynamic torques due to local irregularities in the ablation process will not be considered here. The appropriate differential equation is then ($p = \dot{\varphi}$),

$$I_x\ddot{\varphi} + K_{\text{aero}}\dot{\varphi} - W(\bar{z}\sin\lambda - \bar{y}\cos\lambda) = 0 \qquad \text{(A1)}$$

In order to solve this equation it is necessary to obtain expressions for $\bar{y}$ and $\bar{z}$ as functions of time. Approximate

† Note added in proof: During review of this paper additional tests of prespun Korotherm cones at angle of attack were made. In all cases immediate torques in the direction of initial spin were noted. The mechanism that created the torques for the melting, spinning models at angle of attack is believed to stem from body shape changes arising because of the relatively large thermal expansion characteristics of the Korotherm material rather than from the liquid layer run off per se.

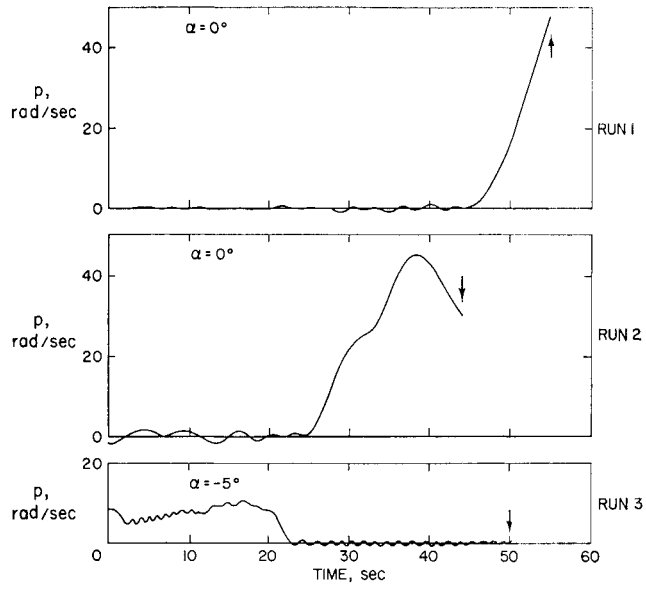

Fig. 13 Roll histories of 30° Korotherm cones.

relationships were derived as follows: the change in cone radius Δr, due to ablation, is assumed to be of the form

$$\Delta r = (x/l)^{-n}[h_0 + h_1\alpha\cos(\theta + \varphi)]t \qquad \text{(A2)}$$

For cones, the following relationships are obtained:

$$\frac{\bar{y}}{r_b} = -\frac{3}{3-n}\left(\frac{h_1\alpha}{r_b}\right)\left(\cos\varphi\int_0^t\cos\varphi dt + \sin\varphi\int_0^t\sin\varphi dt\right) \qquad \text{(A3)}$$

$$\frac{\bar{z}}{r_b} = -\frac{3}{3-n}\left(\frac{h_1\alpha}{r_b}\right)\left(\sin\varphi\int_0^t\cos\varphi dt - \cos\varphi\int_0^t\sin\varphi dt\right) \qquad \text{(A4)}$$

The shape parameter h_1 is to be obtained from consideration of

$$h_1 = (h_1/h_0)h_0 \qquad \text{(A5)}$$

where the ratio h_1/h_0 is to be evaluated experimentally and h_0 either from experiment or estimated by theory. Static tests ($p = 0$) of 10° and 15° metal-tipped camphor models at

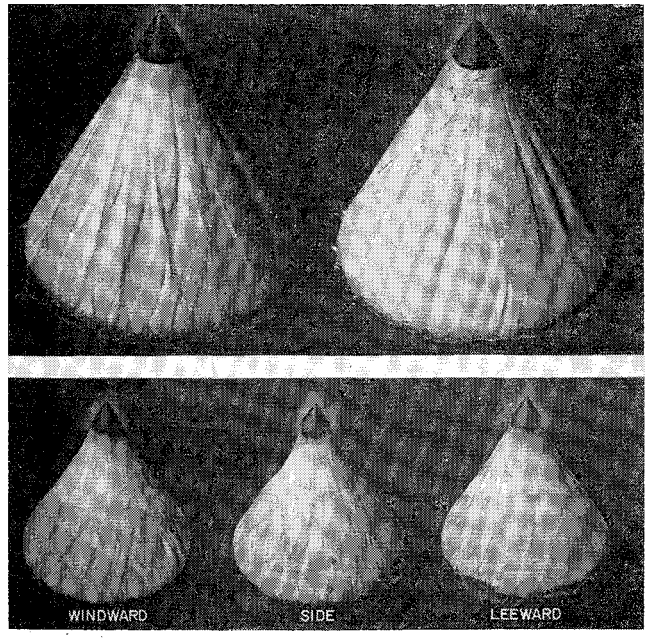

Fig. 14 Postrun photographs of 30° Korotherm cones tested at $\alpha = 0°$ (top) and $\alpha = -5°$ (bottom).

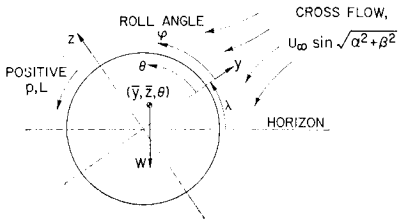

Fig. 15 Nomenclature for weight torque analysis.

$\alpha = 0°$ and 4° indicated that the form of Eq. (A2) is proper for small α in that a cosine variation describes reasonably well the experimental azimuthal variation, and the indicated ablation rates at the cone side meridians agree, within the accuracy of the tests, with measurements at $\alpha = 0°$. A value of approximately $n = 1$ for the exponent was also suggested by the measurements (the data were not sufficiently precise to suggest a preference for the value $n = \frac{4}{5}$ associated with turbulent flow analyses). The parameter h_1/h_0, obtained from

$$\frac{h_1}{h_0} = \frac{1}{\alpha}\left[\frac{(\Delta r/r_b t)_{\theta=0} - (\Delta r/r_b t)_{\theta=\pi/2}}{(\Delta r/r_b t)_{\theta=\pi/2}}\right]$$

is shown in Fig. 16. Since the variation with cone angle σ_c is large, the usefulness of the present rather meager experimental measurements might be enhanced if a suitable normalizing factor could be found. Although the influence of crossflow at the surface on the azimuthal distribution of ablation rate would be difficult to ascertain, the effect of pressure gradient can be approximated. At hypersonic speeds

$$[(\partial P/\partial\alpha)/P]_{\alpha,\theta=0} \sim \mathrm{ctn}\sigma_c$$

and the parameter $(\mathrm{ctn}\sigma_c)^n$ is suggested as the normalizing factor. Again, if $n = 1$, the normalized values are presented in Fig. 16, and the result is the following empirical relationship

$$h_1 = (1.7\ \mathrm{ctn}\sigma_c)h_0 \qquad \text{(A6)}$$

A convenient way to estimate h_0 for cones when $\Delta r/r_b$ is small, and thus difficult to measure accurately, is to apply the approximation

$$h_0/r_b \approx [(2-n)/6][1 - (W_1/W_0)]/t \qquad \text{(A7)}$$

where W_0 is the initial mass of the cone and W_1 is the mass after exposure to the heating environment for time t. Thus, if models are weighed before and after testing, and a suitable value is chosen for n, an approximate average value for h_0 is easily found from Eq. (A7).

Numerical Calculations

Using Eqs. (A6) and (A7) the roll history of an ablating model in the wind tunnel can be estimated numerically. For convenience, the differential equation is expressed in the form

$$\ddot{\varphi} + (K_1 - K_5)\dot{\varphi} + (K_2\cos\lambda)\bar{y}/r_b - (K_2\sin\lambda)\bar{z}/r_b - K_4 = 0$$

where

$$\bar{y}/r_b = -K_3[(\cos\varphi)F + (\sin\varphi)G]$$
$$\bar{z}/r_b = -K_3[(\sin\varphi)F - (\cos\varphi)G]$$

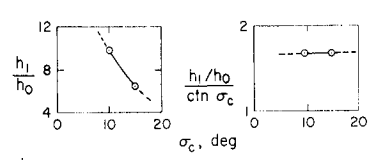

Fig. 16 Experimental values for the ablation parameter h_1/h_0.

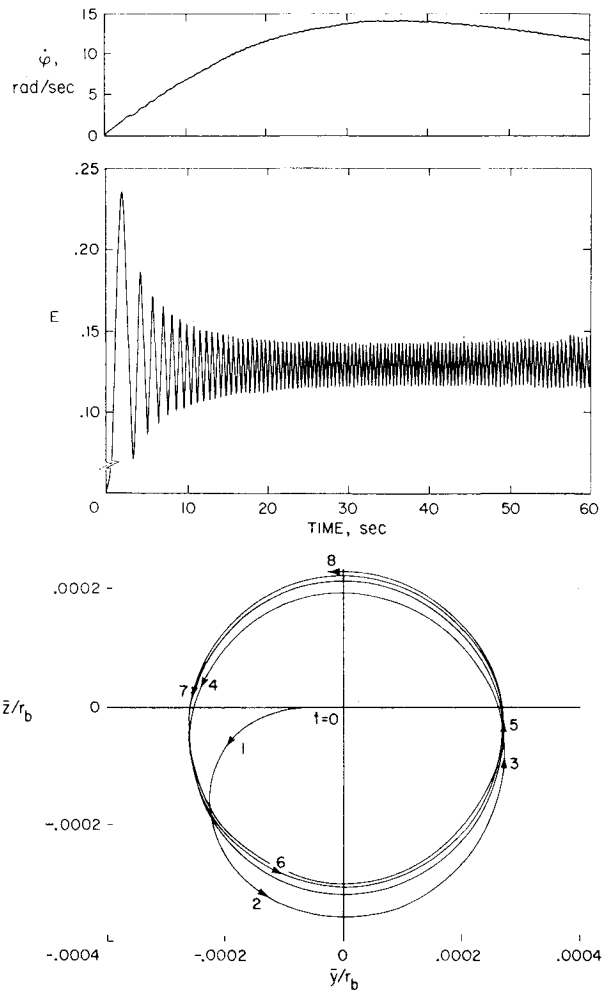

Fig. 17 Numerical solution for an ablating cone; $\lambda = 0$, $K_1 = 0.02 + 0.001t$, $L_2 = 700$, $K_3 = 0.0002$, $K_4 = 0.8$, $K_5 = -0.01$.

and

$$F = \int_0^t (\cos\varphi)d\tau \qquad G = \int_0^t (\sin\varphi)d\tau$$

The aerodynamic damping is represented by $K_1 = K_{\mathrm{aero}}/I_x$; the physical characteristics of the model by $K_2 = r_b(W/I_x)$; the ablation shape changes through $K_3 = [3/(3+n)](h_1/r_b)$; and, finally, the tare moment of the gas bearing is represented by $L_{\mathrm{tare}}/I_x = K_4 + K_5\dot{\varphi}$. A simple numerical technique was programed for solving these equations and an attempt was made to predict the behavior of the model tested in run 1, Fig. 7. An estimate for K_1 was $K_1 = 0.02 + 0.001t$. (The damping increased with test time because the originally smooth surface became increasingly rougher.) The other parameters were evaluated to be $K_2 = 700$, $K_3 = 0.0002$, $K_4 = 0.8$, $K_5 = -0.01$, and $\lambda = 0$. The results of the computation are presented in Fig. 17. Note that the calculated $\dot{\varphi}(t)$ is similar to that for run 1, Fig. 7 ($p = \dot{\varphi}$). In order to understand more clearly the effect of the weight torque, arising from differential ablation due to α, a parameter E, which is proportional to angular momentum,

$$E = \int_0^t [(\sin\lambda)K_2\bar{z}/r_b - (\cos\lambda)K_2\bar{y}/r_b]dt$$

was evaluated and is also shown in Fig. 17. It is evident that the weight torque has a large effect on the roll motion for the first few seconds, but the mean value for E soon becomes essentially constant (averaged over each complete revolution). Thus the small amplitude contribution of the weight torque to the $\dot{\varphi}$ vs t curve can be ignored in this par-

ticular case and the aerodynamic damping may be evaluated directly from the data (neglecting, of course, the first few seconds of data and accounting properly for the tare moment).

References

[1] Williams, E. P., "Experimental Studies of Ablation Surface Patterns and Resulting Roll Torques," AIAA Paper 69-180, New York, 1969.

[2] Chapman, D. R., Larson, H. K., and Anderson, L. A., "Aerodynamic Evidence Pertaining to the Entry of Tektites into the Earth's Atmosphere," TR R-134, 1962, NASA.

[3] Chapman, D. R. and Larson, H. K., "The Lunar Origin of Tektites," TN D-1556, 1963, NASA.

[4] Canning, T. N., Wilkins, M. E., and Tauber, M. E., "Boundary-Phenomena Observed on the Ablated Surfaces of Cones Recovered After Flights at Speeds up to 7 km/sec," CP-19, Vol. 2, 1967, AGARD.

[5] Canning, T. N., Tauber, M. E., and Wilkins, M. E., "Review of Recent Ballistic Range Boundary-Layer Transition Work on Ablated Bodies at Ames," BSD TR-67-123, Vol. III, Sec. 16, 1967, U.S. Air Force.

[6] Larson, H. K., and Mateer, G. G., "Transition Measurements on Cones in Hypersonic Flow and Preliminary Observations of Surface Ablation Grooves," BSD TR 67-213, Vol. III, Sec. 17, 1967, U.S. Air Force.

[7] Canning, T. N., Wilkins, M. E., and Tauber, M. E., "Ablation Patterns on Cones Having Laminar and Turbulent Flows," *AIAA Journal*, Vol. 6, No. 1, Jan. 1968, pp. 174–175.

[8] Larson, H. K. and Mateer, G. G., "Cross-Hatching—A Coupling of Gas Dynamics With the Ablation Process," AIAA Paper 68-670, Los Angeles, Calif., 1968.

[9] Canning, T. N. et al., "Orderly Three-Dimensional Processes in Turbulent Boundary Layers on Ablating Bodies," CP-30, 1968, AGARD.

[10] Laganelli, A. L. and Nestler, D. E., "Surface Ablation Patterns: A Phenomenology Study," *AIAA Journal*, Vol. 7, No. 7, July 1969, pp. 1319–1325.

[11] Tobak, M., "Hypothesis for the Origin of Cross-Hatching," *AIAA Journal*, Vol. 8, No. 2, Feb. 1970, pp. 330–334.

[12] McDevitt, J. B., and Mellenthin, J. A., "Upwash Patterns on Ablating and Nonablating Cones at Hypersonic Speeds," TN D-5346, 1969, NASA.

[13] Ginoux, J. J., "Streamwise Vortices in Laminar Flow," *Recent Developments in Boundary Layer Research*, AGARDograph 97, Pt. I, 1965, pp. 395–422.

[14] Hopkins, E. J., Keating, S. J., Jr., and Bandettini, A., "Photographic Evidence of Streamwise Arrays of Vortices in Boundary-Layer Flow," TN D-328, 1960, NASA.

[15] Nachtsheim, P. R., "Analysis of the Stability of a Thin Liquid Film Adjacent to a High-Speed Gas Stream," TN D-4976, 1969, NASA.

[16] Larson, H. K. and Nachtsheim, P. R., *'Crosshatching' Compressible Turbulent Boundary Layers*, NASA SP 216, 1969, pp. 381–388.